(*Abstract for the 36th International Workshop on Water Waves and Floating Bodies, Seoul, Korea, 2021*)

Numerical Computations of Ship Added Resistance in Time Domain

Xingyu Song[1]*, Rahul Subramanian[2], Xinshu Zhang[1]†, Robert F. Beck[3]

[1]State Key Laboratory of Ocean Engineering, Shanghai Jiao Tong University, Shanghai 200240, China

[2]Department of Ocean Engineering, Texas A&M University, Galveston 77553, USA

[3]Department of Naval Architecture and Marine Engineering, University of Michigan, Ann Arbor MI 48109, USA

Highlights

- The comparison study is conducted between the direct pressure integration method (near-field) and the momentum conservation approach (middle-field) based on both double-body and Neumann-Kelvin linearizations for the evaluation of added resistance.
- The control surface in middle-field method is placed near the hull, and its truncation depth is determined based on the decay of fluid velocities.
- The components and distribution of added resistance in different wavelengths are compared and discussed.

1 Introduction

The accurate prediction of added resistance is critical to ship design and hull form optimization, since it can be up to 15∼30% of the calm water resistance. Moreover, according to the regulatory requirements referring to Energy Efficiency Design Index (EEDI), the EEDI value should be reduced by 30% in comparison with phase 0 (2013∼2014) until year 2025. To correctly estimate this index, the accurate prediction of wave added resistance is of great importance. In general, there are two major methods to compute the added resistance, i.e. near-field method and far-field method. The former approach applies direct pressure integration over the mean wetted hull, while the latter one employs the integration on a control surface in far field based on the momentum conservation formulation (Maruo, 1960). The far-field approach is assumed to have better convergence performance than the near-field method. Besides, there is no need to evaluate the second derivatives of the potential in far-field method. Joncquez *et al.* (2012) studied the added resistance using AEGIR, and compared the results obtained by the forementioned two methods. Later, Pan *et al.* (2016) adopted a new approach named middle-field formulation by applying the momentum conservation principle to a near field volume surrounded by a control surface not far away from the hull. It was shown that the middle-field approach has the same rapid numerical convergence as the far-field method. However, there is little work on the comparison between near-field and middle-field methods and this is the principal focus of this paper.

In the present study, a well-established three-dimensional time-domain seakeeping code (Zhang *et al.*, 2010*a*) employing desingularized source and panel methods is extended to study the added resistance problem. The free surface boundary conditions are applied on the calm water surface, and the body boundary condition is applied on the mean wetted hull surface. The seakeeping model is developed based on the linearizations employing a double-body basis flow or a uniform flow. Both the near-field and middle-field methods are adopted to compute the added resistance in head seas. The containership model S175 is used to validate the proposed model by comparing with experimental data. The comparison is also conducted with the results of body-exact strip theory (Subramanian & Beck, 2019) to analyze the effects of exact body boundary condition. Furthermore, the components and distribution of added resistance are compared and discussed.

2 Mathematical formulation

The vessel is assumed to move with constant speed $\vec{W} = (U, 0, 0)$ in the presence of incident waves (the incident wave amplitude is denoted as A), and may be undergoing unsteady oscillations in its six degrees of freedom. Three right-handed coordinate systems are employed: the $x_0y_0z_0$ system fixed in space, the xyz system fixed to the mean position of the ship (translating with ship forward speed U along the straight track of the ship), and the XYZ system fixed to the ship. The origin of xyz system is located at midship on the mean free surface. The ship is assumed to be a rigid body, and the motion amplitude in translational modes, defined in the xyz system, can be written as

$$\vec{\delta} = \vec{\xi}_T + \vec{\xi}_R \times \vec{X} \tag{1}$$

where $\vec{\xi}_T$ and $\vec{\xi}_R$ are the translation vector (ξ_1, ξ_2, ξ_3) and rotational vector (ξ_4, ξ_5, ξ_6), respectively; $\vec{X} = (X, Y, Z)$ denotes the location on the ship in the XYZ system.

The fluid is assumed to be ideal and the flow irrotational. In the xyz system, the velocity potential $\phi(\vec{x}, t)$ can be introduced to describe the fluid motion such that the fluid velocity can be expressed as the gradient of a potential function, $\vec{V}(\vec{x}, t) = \nabla(-Ux + \phi(\vec{x}, t))$. The potential satisfies the nonlinear boundary value problem (BVP) stated in Zhang *et al.* (2010*a*). The boundary conditions can be linearized using either a

*Presenting author

†xinshuz@sjtu.edu.cn

double-body basis flow or a uniform flow. These two different linearizations are called double-body (DB) and Neumann-Kelvin (NK) linearizations, respectively. The velocity potential ϕ and the free-surface elevation η are decomposed as follows

$$\phi(\vec{x},t) = \Phi(\vec{x}) + \phi_d(\vec{x},t) + \phi_I(\vec{x},t) \tag{2}$$

$$\eta(x,y,t) = \bar{\eta}(x,y) + \eta_d(x,y,t) + \eta_I(x,y,t) \tag{3}$$

where Φ, ϕ_d and ϕ_I denote the basis potential, disturbed wave potential and incident wave potential, respectively; $\bar{\eta}$, η_d and η_I denote the steady, disturbed and incident wave elevations, respectively. The basis potential is assumed to be the main component and its order is $O(1)$, while both disturbed and incident components and their corresponding wave elevations are $O(\epsilon)$, where $\epsilon \ll 1$ denotes a small quantity such as the slenderness of the ship. The mean wave elevation is assumed to be small. By applying Taylor expansions for the instantaneous wave elevation around $z=0$ and the wave-induced motions around the mean wetted hull surface $S_{\bar{B}}$, the linearized boundary conditions can be written as

$$\left(\frac{\partial}{\partial t} - \left(\vec{W} - \nabla\Phi\right)\cdot\nabla\right)\eta_d = \frac{\partial^2\Phi}{\partial z^2}\left(\eta_d + \eta_I\right) + \frac{\partial\phi_d}{\partial z} - \nabla\Phi\cdot\nabla\eta_I \quad \text{on} \quad z=0 \tag{4}$$

$$\left(\frac{\partial}{\partial t} - \left(\vec{W} - \nabla\Phi\right)\cdot\nabla\right)\phi_d = -g\eta_d - \nabla\Phi\cdot\nabla\phi_I \quad \text{on} \quad z=0 \tag{5}$$

$$\frac{\partial\phi_d}{\partial n} = \sum_{j=1}^{6}\left(\frac{\partial\xi_j}{\partial t}n_j + \xi_j m_j\right) - \frac{\partial\phi_I}{\partial n} \quad \text{on} \quad S_{\bar{B}} \tag{6}$$

where $\vec{n}$ is the inward unit normal on the body surface in xyz system; n_j denote the generalized normal vectors; m_j represent the m-terms including the effects of the interaction between the steady and unsteady flows.

By applying Green's theorem, with employing desingularized sources above the calm water surface and constant-strength panels on the hull, the velocity potential can be written as (Zhang *et al.*, 2010*b*)

$$\phi(\vec{x}) = \sum_{N_F} G(\vec{x};\vec{x}')\sigma(\vec{x}') + \iint_{S_{\bar{B}}} G(\vec{x};\vec{x}')\sigma(\vec{x}')\mathrm{d}s \tag{7}$$

where $G = 1/r(\vec{x};\vec{x}')$; σ is the source strength on the boundaries; N_F is the number of desingularized sources distributed above the calm water surface.

The body-exact strip theory is carried out in time domain and developed for maneuvering problem in waves. The exact body boundary condition is applied on the instantaneous wetted hull surface. In addition, the radial basis function is employed to compute all the x-derivatives and acceleration potential for ϕ_t terms. Besides, the usual strip theory forward speed corrections are made to the potential flow solution and the viscous effects are taken into consideration.

2.1 Near-field approach

By applying the Bernoulli's equation and performing Taylor's expansion for both hydrodynamic pressure and instantaneous wetted body surface, the second-order force $\vec{F}_2$ can be obtained

$$\begin{aligned}
\vec{F}_2 \;=\; & -\rho\int_{WL}\left(-\vec{W}\cdot\nabla\Phi + \frac{1}{2}\nabla\Phi\cdot\nabla\Phi\right)\eta_r\vec{\xi}_R\times\vec{N}\mathrm{d}l - \rho\int_{WL}\vec{\delta}\cdot\nabla\left(-\vec{W}\cdot\nabla\Phi + \frac{1}{2}\nabla\Phi\cdot\nabla\Phi\right)\eta_r\vec{N}\mathrm{d}l \\
& + \int_{WL}\frac{1}{2}\rho g\eta_r^2\vec{N}\mathrm{d}l - \rho\iint_{S_{\bar{B}}}\left[H\vec{X}\cdot\nabla\left(gZ - \vec{W}\cdot\nabla\Phi + \frac{1}{2}\nabla\Phi\cdot\nabla\Phi\right)\right]\vec{N}\mathrm{d}s - \rho\iint_{S_{\bar{B}}} gZH\vec{N}\mathrm{d}s \\
& -\rho\iint_{S_{\bar{B}}}\vec{\delta}\cdot\nabla\left[\frac{\partial(\phi_d+\phi_I)}{\partial t} - (\vec{W}-\nabla\Phi)\cdot\nabla(\phi_d+\phi_I)\right]\vec{N}\mathrm{d}s - \rho\iint_{S_{\bar{B}}}\frac{1}{2}\left[\nabla(\phi_d+\phi_I)\cdot\nabla(\phi_d+\phi_I)\right]\vec{N}\mathrm{d}s \\
& -\rho\iint_{S_{\bar{B}}}\left[g\left(\xi_3 + \xi_4 Y - \xi_5 X\right) + \frac{\partial(\phi_d+\phi_I)}{\partial t} - (\vec{W}-\nabla\Phi)\cdot\nabla(\phi_d+\phi_I)\right]\vec{\xi}_R\times\vec{N}\mathrm{d}s \\
& -\rho\iint_{S_{\bar{B}}}\left(-\vec{W}\cdot\nabla\Phi + \frac{1}{2}\nabla\Phi\cdot\nabla\Phi\right)H\vec{N}\mathrm{d}s - \rho g\iint_{S_{\bar{B}}}\left[\vec{\delta}\cdot\nabla\left(-\vec{W}\cdot\nabla\Phi + \frac{1}{2}\nabla\Phi\cdot\nabla\Phi\right)\right]\vec{\xi}_R\times\vec{N}\mathrm{d}s
\end{aligned} \tag{8}$$

where WL denotes the mean waterline; $\vec{N}$ is the unit normal vector into the hull in XYZ system; η_r is defined as the relative wave elevation which accounts for the time-dependent instantaneous ship motion; H is the matrix of transformation and its expression can be found in WAMIT (2016). The added resistance R_{aw} can be obtained by taking the average of the longitudinal component of $\vec{F}_2$ with respect to time.

2.2 Middle-field approach

The momentum conservation principle is applied to a near field volume Ω bounded by a closed surface S_Ω which consists of the instantaneous free surface S_F, the instantaneous wetted hull surface S_B, the bottom surface S_0 and the vertical control surface S_{CS}. The control surface is near the hull and shares the same speed $\vec{W}$ with ship. In the $x_0y_0z_0$ system, the rate of change of linear momentum in the volume Ω is

$$\frac{\mathrm{d}\vec{M}}{\mathrm{d}t} = \iiint_\Omega \rho\nabla\phi\mathrm{d}\tau = \rho\iiint_\Omega\frac{\mathrm{d}}{\mathrm{d}t}\nabla\phi\mathrm{d}\tau + \rho\iint_{S_\Omega}\nabla\phi\left(\vec{W}_{S_\Omega}\cdot\vec{n}_{S_\Omega}\right)\mathrm{d}s \tag{9}$$

where $\vec{W}_{S_\Omega}$ represents the velocity of the surface S_Ω in the $x_0y_0z_0$ system; $\vec{n}_{S_\Omega}$ denotes the unit normal vector out of the surface S_Ω. By applying the Galilean transformation, Eqn.(9) can be expressed in the xyz system as

$$\frac{\mathrm{d}\vec{M}}{\mathrm{d}t} = \rho\iiint_\Omega\left(\frac{\partial}{\partial t} - \vec{W}\cdot\nabla\right)\nabla\phi\mathrm{d}\tau + \rho\iint_{S_\Omega}\nabla\phi\left(\vec{W}_{S_\Omega}\cdot\vec{n}_{S_\Omega}\right)\mathrm{d}s \tag{10}$$

After employing the Euler equation, the first Green identity and divergence theorem, the expression of second-order force can be written as

$$\begin{aligned}\vec{F}_2(t) &= -\frac{\rho g}{2}\int_{C_d}(\eta_I+\eta_d)^2\vec{n}_c\mathrm{d}l-\rho\int_{C_d}\left[\nabla\Phi\left(\nabla\left(\phi_d+\phi_I\right)\cdot\vec{n}_c\right)+\nabla(\phi_d+\phi_I)\left((\nabla\Phi-\vec{W})\cdot\vec{n}_c\right)\right](\eta_I+\eta_d)\,\mathrm{d}l\\ &\quad\frac{\rho}{2}\iint_{S_d}\left[\nabla(\phi_d+\phi_I)\cdot\nabla(\phi_d+\phi_I)\right]\vec{n}_c\mathrm{d}s-\rho\iint_{S_d}\nabla(\phi_d+\phi_I)\left[\nabla(\phi_d+\phi_I)\cdot\vec{n}_c\right]\mathrm{d}s \qquad (11)\end{aligned}$$

where $\vec{n}_c$ denotes the unit normal vector out of the control surface; S_d is the control surface truncated at a finite depth; C_d is the intersection line of S_d with the $z=0$ plane. It should be noted that, different from the far-field method in which the control surface should be placed at least 3.5 times the incoming wavelength λ away from the hull (Seo *et al.*, 2013), the middle-field approach has no such strict requirement for the size of computational domain, since the control surface can be set close to the ship. In the middle-field approach, the boundary of computational domain can be set about $1L$ away from the ship.

3 Results and discussion

Head sea conditions are considered for all analyses presented in this paper. The time step is one percent of the encounter period for both speed conditions, with Froude number (Fn) at 0.2 and 0.25. There are 29×8=232 panels on the wetted hull, 2856 panels on the free surface and 1250 panels on the control surface. The computational domain on the free surface extends 1.5 times the ship length L in the y-direction, $0.5L$ upstream and $1L$ downstream. The open boundary condition is applied to all the boundaries of the computational domain, except the lateral boundary of the free surface where a numerical damping beach is applied to prevent the wave reflection and to satisfy the radiation condition. The control surface is defined as half the elliptic cylindrical surface and its dimensions in the x and y directions are set with $1.1L$ and 1.4 times ship breadth B, respectively. The truncation depth of the control surface is equal to one incoming wavelength where the fluid velocity is almost negligible. The distributions of fluid velocities caused by the disturbed waves along the vertical direction are shown in Fig.1. We can see that the velocities in three directions all have attenuated exponentially to zero at $z=-\lambda$. What's interesting though is that their rates of decay are different. The exponential decay factor for the longitudinal velocity is roughly the wavenumber of the incoming wave k_I, while those for the transverse and vertical velocities are approximately the wavenumber corresponding to the encountered wave frequency $k_e=(\sqrt{k_Ig}+k_IU)^2/g$. In addition, it is found that the fluid velocities in far field also have different rates of decay in vertical direction.

The vertical motions and added resistance for S175 with different speeds are illustrated in Fig.2. As shown in Fig.2(a), (b), (d) and (e), the body-exact strip theory gives the best prediction for vertical motions, which reflects the importance of using the exact wetted surface for the pressure integration over the hull. The overall tendencies of the vertical motions by NK and DB linearizations are similar and show good agreement with experimental data, except that both heave and pitch motion responses are somehow overestimated in the resonance region ($1.0<\lambda/L<1.7$). Around the peak value frequency, DB linearization gives better motion results, since it takes the effect of interaction between steady and unsteady flows into account. As shown in Fig.2(c) and (f), the added resistances obtained by a DB linearization are also better than those by NK, especially for the near-field method. As for the added resistance obtained by near-field method (NK), the peak value frequency is shifted to the long wave region. As for the added resistance obtained by middle-field method (NK), they are overestimated in short waves while underestimated in long waves. The added resistance obtained by near-field method (DB) agree well with the experimental data at $Fn=0.2$. However, as the Froude number increases, the added resistance is slightly underestimated by near-field method (DB) around the peak value frequency ($0.9<\lambda/L<1.3$). This may be because the DB linearization is regarded as a slow-ship linearization. It should be noted that, in the two cases with different Froude numbers, the middle-field method based on DB linearization gives better results than near-field method. As can be seen in Fig.2(c) and (f), the body-exact strip theory offers good estimation for added resistance in intermediate wavelength waves, but it overestimates in long waves.

The distribution and different components of added resistance are shown in Fig.3. As illustrated in Fig.3(a), the main contribution to the added resistance comes from the waterline integral, while the pressure integration over the mean wetted hull surface has negative effects on added resistance. As shown in Fig.3(b), the added resistance from the pressure integration above and below the waterline are both mainly in stem region. In addition, Fig.3(c) shows that the stem region affected by the added resistance from waterline integration gets smaller, as wavelength increases. Meanwhile, the peak value position moves towards the bow.

References

Fonseca, N. & Guedes Soares, C. 2004 *Journal of Ship Research* **48** (2), 118–147.
Fujii, H. & Takahashi, T. 1975 In *Proceedings of the 14th ITTC, Ottawa, Canada*, pp. 351–360.
Joncquez, S. A., Andersen, P. & Bingham, H. B. 2012 *Journal of Ship Research* **56** (2), 106–119.
Maruo, H. 1960 *Journal of Ship Research* **4** (3), 1–10.
Nakamura, S. & Naito, S. 1977 *Journal of the Society of Naval Architects of Japan* **15**, 24–48.
Pan, Z., Vada, T. & Han, K. 2016 In *Proceedings of the 35th OMAE2016-54353, Busan, South Korea*.
Seo, M. G., Park, D. M., Yang, K. K. & Kim, Y. 2013 *Ocean Engineering* **73**, 1–15.
Subramanian, R. & Beck, R. F. 2019 In *Proceedings of the 38th OMAE2019-96441, Glasgow, Scotland, UK*.
Tasaki, R. & Mizoguchi, S. 1981 In *Proceedings of the 16th ITTC, Leningrad, USSR*, pp. 123–127.
WAMIT, INC. 2016 User Manual for WAMIT Version 7.2. www.wamit.com/manual.htm.
Zhang, X., Bandyk, P. & Beck, R. F. 2010*a* *Applied Ocean Research* **32** (4), 471–482.
Zhang, X., Bandyk, P. & Beck, R. F. 2010*b* *Journal of Ship Research* **54** (2), 79–94.

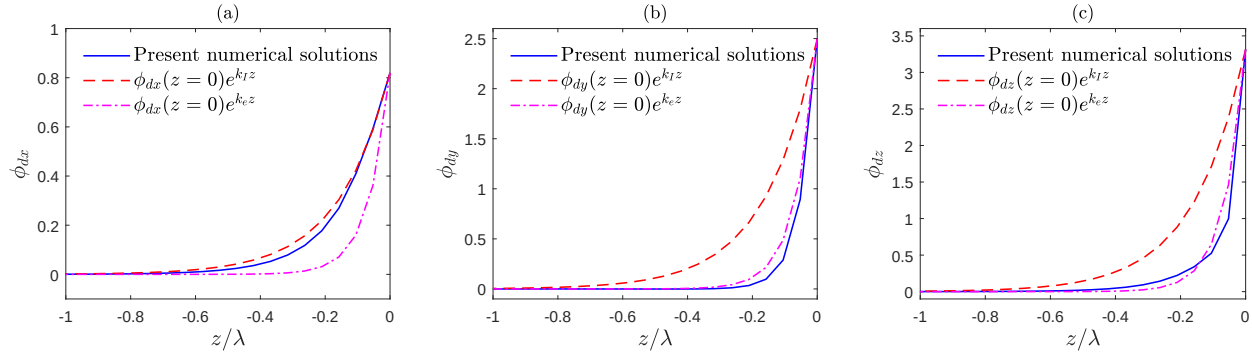

Figure 1: Distribution of fluid velocities caused by disturbed waves along the vertical direction. The shared horizontal position of the probes is $(-0.43L, -0.06L)$ near the stern on the control surface. (a) Longitudinal velocity; (b) Transverse velocity; (c) Vertical velocity.

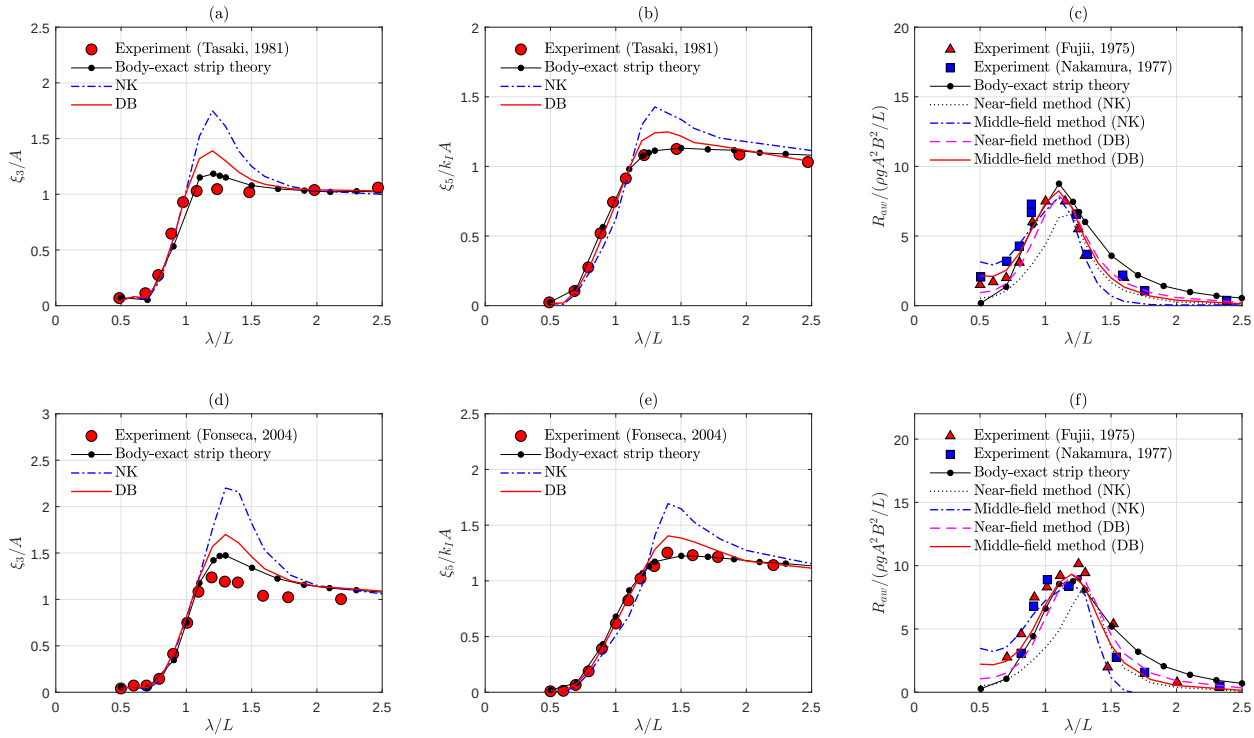

Figure 2: Comparison of vertical motions and added resistance on S175 containership in head seas by NK, DB and body-exact strip theory. (a) Heave RAOs at Fn=0.2; (b) Pitch RAOs at Fn=0.2; (c) Added resistance at Fn=0.2; (d) Heave RAOs at Fn=0.25; (e) Pitch RAOs at Fn=0.25; (f) Added resistance at Fn=0.25.

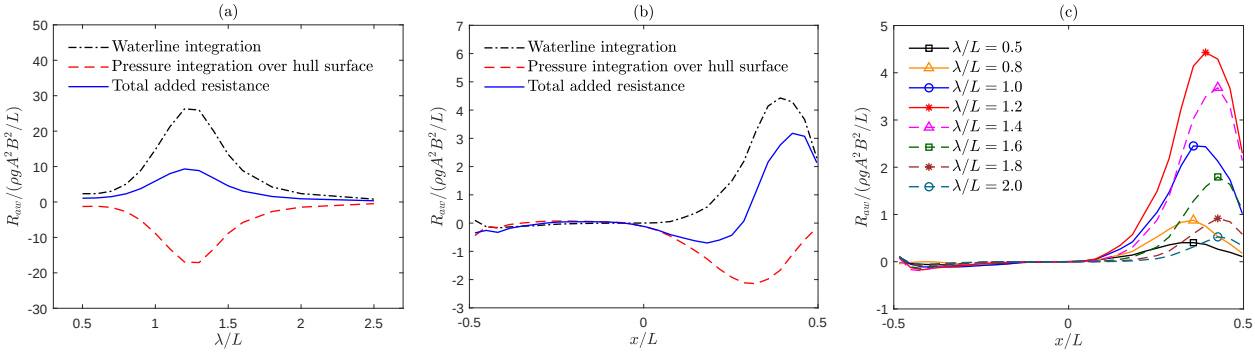

Figure 3: The components and distribution of added resistance on S175 containership at Fn=0.25 in head seas by near-field method (DB). (a) Comparison of added resistance from waterline integral and pressure integration over the mean wetted hull surface in Eqn.(8); (b) Comparison of added resistance distribution in longitudinal direction contributed by waterline integral and pressure integration over hull surface for λ/L=1.2; (c) Comparison of added resistance distribution in longitudinal direction contributed by waterline integration for different wavelengths.